INTERNATIONAL JOURNAL FOR NUMERICAL METHODS IN FLUIDS, VOL. 5, 443–462 (1985)

APPLICATION OF THE DORODNITSYN FINITE ELEMENT METHOD TO SWIRLING BOUNDARY LAYER FLOW

C. A. J. FLETCHER

Department of Mechanical Engineering, University of Sydney, NSW 2006, Australia

SUMMARY

The Dorodnitsyn finite element method for turbulent boundary layer flow with surface mass transfer is extended to include axisymmetric swirling internal boundary layer flow. Turbulence effects are represented by the two-layer eddy viscosity model of Cebeci and Smith[1] with extensions to allow for the effect of swirl. The method is applied to duct entry flow and a 10 degree included-angle conical diffuser, and produces results in close agreement with experimental measurements with only 11 grid points across the boundary layer. The introduction of swirl ($w_e/u_e = 0{\cdot}4$) is found to have little effect on the axial skin friction in either a slightly favourable or adverse pressure gradient, but does cause an increase in the displacement area for an adverse pressure gradient. Surface mass transfer (blowing or suction) causes a substantial reduction (blowing) in axial skin friction and an increase in the displacement area. Both suction and the adverse pressure gradient have little influence on the circumferential velocity and shear stress components. Consequently in an adverse pressure gradient the flow direction adjacent to the wall is expected to approach the circumferential direction at some downstream location.

KEY WORDS Turbulent flow Boundary Layer Flow Swirl Surface Mass Transfer Finite Element Method

1. INTRODUCTION

Boundary layer flows have been computed accurately since the 1968 Stanford Conference.[2] Two dimensional and axisymmetric boundary layer solutions for the velocity components, u and v, are typically obtained with x and y (or r) as independent variables.

Particularly when computing turbulent boundary layers a large number of points are required close to the surface (Figure 1) to accurately represent the velocity profile. A more efficient way of representing the velocity profile is to replace the normal co-ordinate, y or r, with the longitudinal or axial velocity component, u, as an independent variable. Consequently grid points at equal intervals of u are automatically clustered close to the surface where the solution is changing most rapidly.

Both the Dorodnitsyn[3] and Crocco boundary layer formulations make use of u as an independent variable. However the Dorodnitsyn formulation includes an integration over the normal co-ordinate which permits a Galerkin[4] interpretation of the formulation and the subsequent development of a modified finite element method.

The use of the longitudinal velocity component, u, as an independent variable has other advantages. First a finite domain in the normal direction replaces an infinite domain in the y direction. Secondly the growth of the boundary layer in the longitudinal direction is captured

0271–2091/85/050443–20$02.00

Received 4 May 1984
Revised 5 November 1984

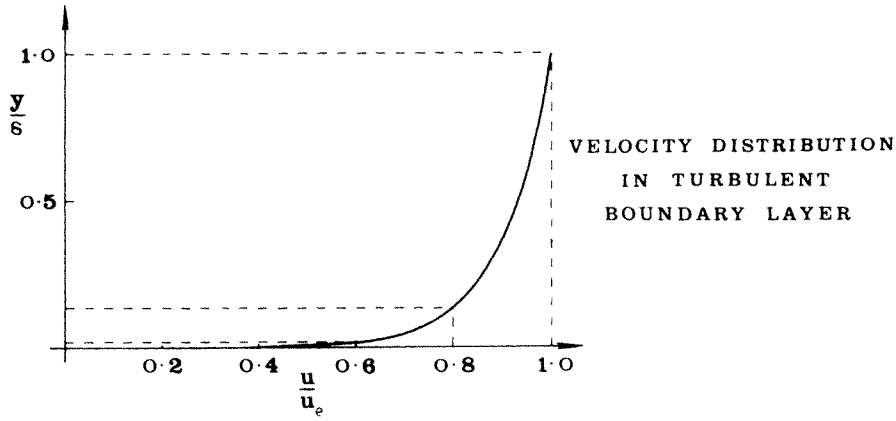

Figure 1. Turbulent boundary layer velocity profile

automatically. In physical space it would be necessary to have an irregular grid, with an inherent loss of accuracy, or to redefine the grid in the normal direction at discrete intervals downstream.

The Dorodnitsyn formulation possesses other benefits. In two dimensions the particular nature of the integral formulation avoids the specific appearance of the normal velocity component, v, as a dependent variable. The solution for the normal velocity can be recovered, subsequently, if required. The Dorodnitsyn formulation treats the non-dimensional normal gradient of the velocity component, u, as the dependent variable. As a result the skin friction can be computed very accurately.

Originally the Dorodnitsyn formulation was developed to apply the method of integral relations[5] to boundary layer flows. Subsequently it has been possible to reinterpret[4,6] the Dorodnitsyn boundary layer formulation as a Galerkin method in both spectral and finite element forms.

The Dorodnitsyn spectral formulation has been applied to incompressible[7] and compressible[8] laminar boundary layer flows. The Dorodnitsyn spectral formulation has also been applied to incompressible[9,10] and compressible[11] turbulent boundary layer flows.

The Dorodnitsyn finite element formulation has been applied to laminar incompressible flow[12] and shown to yield an accurate and very economical algorithm. Using quadratic elements the Dorodnitsyn finite element formulation is approximately five times more efficient than a conventional finite difference formulation.

Numerical experiments indicate that the method converges like $(\Delta u^2, \Delta x)$ whether linear or quadratic elements are used. However of greater importance is the fact that solutions of high accuracy are obtained on a relatively coarse grid.

The Dorodnitsyn finite element formulation has been applied to incompressible turbulent boundary layer flow[10] and shown to be about ten times more efficient than a representative finite difference package. A large component of this superior efficiency comes from only requiring about a third to a quarter of the number of grid points in the normal direction to accurately represent the velocity profile. Developments of the Dorodnitsyn finite element formulation have been applied to compressible turbulent boundary layers[11] and to turbulent boundary layers with mass transfer in the normal direction at the wall.[13]

Here the Dorodnitsyn finite element formulation is applied to swirling internal boundary layer flow for which mass transfer at the wall may also occur.

The background to this problem is associated with the flow through diffuser-augmented wind

turbines which have been shown to be well-suited[14] to the generation of electricity from jet-stream winds.[15,16] To obtain the optimum performance from diffuser-augmented wind turbines it is necessary to prevent separation of the flow from the diffuser wall. It is known that the deliberate addition of swirl to the flow helps to delay separation and improve pressure recovery.[17]

The rest of this paper is arranged as follows. In Section 2 the Dorodnitsyn formulation for two-dimensional boundary layer flow is described briefly and a modified finite element interpretation is provided. The extension of the method to handle internal swirling boundary layer flows is described in Section 3. This requires consideration of the circumferential momentum equation, the radial pressure gradient and specific treatment of the eddy viscosity concept to represent the effects of turbulence on the flow development.

The present formulation is applied to swirling duct and conical diffuser flows in Section 4 and the competing influences of swirl and wall injection on the boundary layer development are assessed.

2. DORODNITSYN FINITE ELEMENT FORMULATION

In this section the Dorodnitsyn[3] boundary layer formulation is derived for two-dimensional incompressible turbulent boundary layer flow. Subsequently a modified Galerkin finite element method[4] is developed. In the present paper this will be referred to as the Dorodnitsyn finite element (DOROD-FEM) method.

2.1. Dorodnitsyn boundary layer formulation

Given a characteristic length, L, and velocity U_∞, the non-dimensional equations governing steady two-dimensional incompressible turbulent boundary layer flow can be written as

$$\partial u/\partial x + \partial v/\partial y = 0, \tag{1}$$

and

$$u\partial u/\partial x + v\partial u/\partial y = u_e \mathrm{d}u_e/\mathrm{d}x + \frac{1}{Re}\partial\{(1 + \nu_T/\nu)\partial u/\partial y\}/\partial y, \tag{2}$$

where $u_e(x)$ is the known velocity at the outer edge of the boundary layer. The Reynolds number, $Re = U_\infty L/\nu$. In equation (2) ν_T is the eddy viscosity such that the Reynolds stress, $-\overline{\rho u'v'}$ is replaced by $\nu_T \partial u/\partial y$. The equation system, (1) and (2), is parabolic and requires both initial conditions.

$$u(x_0, y) = u_i(y) \quad \text{and} \quad v(x_0, y) = v_i(y), \tag{3}$$

and boundary conditions,

$$u(x, 0) = 0, \quad v(x, 0) = v_w \quad \text{and} \quad u(x, \infty) = u_e(x). \tag{4}$$

In equation (4) v_w is the (prescribed) normal velocity at the wall.

The Dorodnitsyn boundary layer formulation can be introduced in two stages. In the first stage new independent variables (ξ, η) are introduced,

$$\xi = x \quad \text{and} \quad \eta = Re^{1/2} u_e y,$$

and also new velocity components,

$$u' = u/u_e, \quad v' = Re^{1/2} v/u_e \quad \text{and} \quad v'' = u_e v' + \eta u'\{\mathrm{d}u_e/\mathrm{d}\xi\}/u_e.$$

Equations (1)–(4) become

$$\partial u'/\partial \xi + \partial v''/\partial \eta = 0, \tag{5}$$

$$u'\partial u'/\partial \xi + v''\partial u'/\partial \eta = \{\mathrm{d}u_e/\mathrm{d}\xi\}/u_e + \partial\{(1 + \nu_T/\nu)\partial u'/\partial \eta\}/\partial \eta \tag{6}$$

with auxiliary conditions

$$u' = 0, \quad v'' = Re^{1/2} v_w/u_e \quad \text{at} \quad \eta = 0 \quad \text{and} \quad u' = 1 \quad \text{at} \quad \eta = \infty. \tag{7}$$

A weighted combination of equations (5) and (6) is formed as

$$f_k(u') \times \text{equation (5)} + \{\mathrm{d}f_k(u')/\mathrm{d}u'\} \times \text{equation (6)} = 0,$$

where $f_k(u')$ is a general weight (test) function whose specific form will be indicated below. The weighted combination has the form (after dropping the superscript ′)

$$\partial(u f_k)/\partial \xi + \partial(v'' f_k)/\partial \eta = [\{\mathrm{d}u_e/\mathrm{d}\xi\}/u_e]\mathrm{d}f_k/\mathrm{d}u(1 - u^2) + u_e \mathrm{d}f_k/\mathrm{d}u\partial\{(1 + \nu_T/\nu)\partial u/\partial \eta\}/\partial \eta. \tag{8}$$

An integration is made with respect to η. This gives

$$\frac{\partial}{\partial \xi}\left\{\int_0^\infty u f_k \,\mathrm{d}\eta\right\} + |v'' f_k|_0^\infty = |\{\mathrm{d}u_e/\mathrm{d}\xi\}/u_e| \int_0^\infty \mathrm{d}f_k/\mathrm{d}u(1 - u^2)\mathrm{d}\eta + u_e \int_0^\infty \frac{\mathrm{d}f_k}{\mathrm{d}u}\frac{\partial}{\partial \eta}\left\{\left(1 + \frac{\nu_T}{\nu}\right)\frac{\partial u}{\partial \eta}\right\}\mathrm{d}\eta. \tag{9}$$

The weight function, f_k, is required to satisfy $f_k(\infty) = 0$.

In the second stage of the Dorodnitsyn formulation, new dependent variables are introduced by

$$\mathrm{T} = 1/\Theta = \partial u/\partial \eta, \tag{10}$$

and the variable of integration in equation (9) is changed from η to u. The result is

$$\frac{\partial}{\partial \xi}\left\{\int_0^1 u f_k \Theta \,\mathrm{d}u\right\} - Re^{1/2} u_e F |f_k|_{u=0} = |\{\mathrm{d}u_e/\mathrm{d}\xi\}/u_e| \int_0^1 \frac{\mathrm{d}f_k}{\mathrm{d}u}(1 - u^2)\Theta \,\mathrm{d}u + u_e \int_0^1 \frac{\mathrm{d}f_k}{\mathrm{d}u}\frac{\partial}{\partial u}\{(1 + \nu_T/\nu)\mathrm{T}\}\,\mathrm{d}u, \tag{11}$$

where the (prescribed) mass transfer parameter, $F = v_w/u_e$. Equation (11) is the Dorodnitsyn formulation for turbulent boundary layer flow. In equation (11), ξ and u are independent variables and the unknown normal velocity, v, does not appear explicitly.

The solution of equation (11) requires specification of the form of the approximate solution for T and Θ and the weight function, $f_k(u)$. Different choices lead to the method of integral relations,[5] the Dorodnitsyn spectral formulation[4] and the Dorodnitsyn finite element formulation (see next section).

2.2. *Finite element formulation*

Approximate (trial) solutions for Θ and $(1 + \nu_T/\nu)\mathrm{T}$ are introduced as

$$\Theta = \sum_{j=1}^{M} \{(N_j(u)/(1 - u)\}\theta_j(\xi), \tag{12}$$

and

$$(1 + \nu_T/\nu)\mathrm{T} = \sum_{j=1}^{M} \{(1 - u)N_j(u)\}\{(1 + \nu_T/\nu)\tau(\xi)\}_j, \tag{13}$$

where $N_j(u)$ are one-dimensional shape functions,[18] either linear or quadratic. The additional factor $(1-u)$ is introduced to give T and Θ the correct physical behaviour at the outer edge of the boundary layer. Prescribing separate approximate solutions for T and Θ leads to a more concise and economical algorithm. However it prevents equation (10) from being satisfied except at the nodes, $\tau_j = 1/\theta_j$ or in the limit $M \to \infty$.

It is clear from equation (13) that the approximate solution has been introduced for the group of terms, $[(1+\nu_T/\nu)T]$. This is a particular application of the group finite element formulation.[20] For turbulent boundary layer flow the eddy viscosity is a complicated function of the normal coordinate (see Section 3.3). The introduction of the group formulation, equation (13), permits ν_T to be evaluated at the nodes only. This makes a substantial contribution to the overall economy, and hence the computational efficiency, of the present method. The superior computational efficiency is a major feature of the Dorodnitsyn finite element boundary layer method.[10,12]

The weight function is defined by

$$f_k(u) = (1-u)N_k(u), \tag{14}$$

and this form satisfies the requirement, $f(1) = 0$, introduced after equation (9). Equations (12)–(14) are substituted into equation (11) and produce a modified Galerkin formulation.[4] Evaluation of the various integrals produces the following system of ordinary differential equations for the nodal values τ_j and θ_j:

$$\sum_j \mathrm{CC}_{kj}\frac{\mathrm{d}\theta_j}{\mathrm{d}\xi} = Re^{1/2}u_e F\delta_{1k} + [\{\mathrm{d}u_e/\mathrm{d}\xi\}/u_e]\mathrm{EF}_{kj}\theta_j + u_e\sum_j \mathrm{AA}_{kj}(1+\nu_T/\nu)_j\tau_j, \tag{15}$$

where $\delta_{1k} = 1$ if $k = 1$ and $\delta_{1k} = 0$ if $k \neq 1$. The algebraic coefficients in equation (15) are evaluated, once and for all, from

$$\mathrm{CC}_{kj} = \int_0^1 N_j N_k u\,\mathrm{d}u, \quad \mathrm{EF}_{kj} = \int_0^1 N_j\left\{\frac{\mathrm{d}N_k}{\mathrm{d}u}(1-u) - N_k\right\}(1+u)\mathrm{d}u,$$

and

$$\mathrm{AA}_{kj} = \int_0^1 \left\{\frac{\mathrm{d}N_j}{\mathrm{d}u}(1-u) - N_j\right\}\left\{\frac{\mathrm{d}N_k}{\mathrm{d}u}(1-u) - N_k\right\}\mathrm{d}u. \tag{16}$$

An efficient implicit marching algorithm is constructed from equation (15) as follows. First equation (15) is approximated by

$$\sum \mathrm{CC}_{kj}(\alpha\Delta\theta_j^{n+1} + (1-\alpha)\Delta\theta_j^n) = \Delta\xi(\beta\mathrm{RHS}^{n+1} + (1-\beta)\mathrm{RHS}^n). \tag{17}$$

where n denotes the downstream location, α and β are relaxation parameters, $\Delta\theta_j^{n+1} = \theta_j^{n+1} - \theta_j^n$ and RHS is the right-hand side of equation (15). A linear system of equations for $\Delta\theta_j^{n+1}$ is obtained, after linearizing RHS^{n+1} about the downstream location, ξ_n, as

$$\sum_j \mathrm{CCC}_{kj}\Delta\theta_j^{n+1} = P_k, \tag{18}$$

where

$$\mathrm{CCC}_{kj} = \alpha\mathrm{CC}_{kj} - \beta\Delta\xi|[\{\mathrm{d}u_e/\mathrm{d}\xi\}/u_e]^{n+1}\mathrm{EF}_{kj} - u_e^{n+1}\mathrm{AA}_{kj}G_j^n|,$$
$$G_j^n = |(1+\nu_T/\nu)\tau^2 - \{\partial(\nu_T/\nu)/\partial\theta\}\tau|_j^n,$$

and

$$P_k = \Delta\xi|Re^{1/2}u_e^{n,\beta}F\delta_{1k} + [\{\mathrm{d}u_e/\mathrm{d}\xi\}/u_e]^{n,\beta}\sum_j \mathrm{EF}_{kj} + u_e^{n,\beta}\sum_j \mathrm{AA}_{kj}(1+\nu_T/\nu)_j^n\tau_j^n| - (1-\alpha)\sum_j \mathrm{CC}_{kj}\Delta\theta_j^n. \tag{19}$$

In equation (19) the superscript n, β denotes that the term is evaluated at $\xi_n + \beta\Delta\xi$.

The system of equations, (18), is tridiagonal for linear shape functions and pentadiagonal for quadratic shape function. A generalized Thomas algorithm[4] is available to take account of the varying bandwidth of CCC associated with midside and corner nodes when quadratic shape functions are used.

Equation (18) is marched downstream without iteration at each location, ξ_n. Although numerical convergence results[12] indicate that the scheme is accurate to $O(\Delta\xi)$ for $\alpha = 1$ and $\beta = 0{\cdot}6$, it has produced solutions in good agreement with known exact and experimental results with no restriction on the downstream step-size, $\Delta\xi$.

The above algorithm has been applied to laminar,[12] turbulent[10] and turbulent wall-injection[13] boundary layer flows. A feature of the algorithm is that is produces accurate results with typically 11 points across the boundary layer, but with considerable economy. For representative turbulent boundary layer flows the above algorithm (DOROD-FEM) is typically ten times more economical[10] than a representative finite difference package, STAN5,[19] while being equally accurate. The features that contribute to this superior computational efficiency are discussed by Fletcher and Fleet.[10]

3. SWIRLING INTERNAL BOUNDARY LAYER FLOW

In this section the equations of motion governing axisymmetric swirling internal boundary layer flow are manipulated to give the corresponding Dorodnitsyn equations. Subsequently a modified Galerkin finite element interpretation of the Dorodnitsyn equations is developed and the turbulence model for swirling boundary layer flow described.

3.1. Equation of motion and the Dorodnitsyn formulation

The non-dimensional equations of motion governing swirling internal boundary layer flow can be written in polar co-ordinates $(x, r, \phi; u, v, w)$ as

$$\frac{\partial}{\partial x}(ru) + \frac{\partial}{\partial r}(rv) = 0, \tag{20}$$

$$ru\frac{\partial u}{\partial x} + rv\frac{\partial u}{\partial r} = -r\frac{\partial p}{\partial x} + \frac{1}{Re}\frac{\partial}{\partial r}\{r(1 + v_x/v)\partial u/\partial r\}, \tag{21}$$

$$\partial p/\partial r = w^2/r, \tag{22}$$

$$ru\partial w/\partial x + rv\partial w/\partial r + vw = \frac{1}{Re}\frac{\partial}{\partial r}\{r(1 + v_\phi/v)\partial w/\partial r\}. \tag{23}$$

In equations (20) to (23) lengths have been non-dimensionalized by L, velocities by U_∞ and the Reynolds number, $Re = U_\infty L/v$. The terms v_x and v_ϕ are the axial and circumferential eddy viscosities which are introduced to represent the Reynolds shear stresses. In equations (20)–(23) the dependent variables, u, v, w and p, are functions of x and r only; there is no circumferential dependence.

The equation system (20)–(23), is parabolic and requires corresponding initial conditions,

$$u(x_0, r) = u_i(r), \quad v(x_0, r) = v_i(r), \quad w(x_0, r) = w_i(r), \tag{24}$$

and boundary conditions,

$$\begin{aligned} &u(x, r_w) = 0, \quad v(x, r_w) = v_w, \quad w(x, r_w) = 0, \\ &u(x, r_e) = u_e(x), \quad w(x, r_e) = w_e(x), \quad p(x, r_e) = p_e(x). \end{aligned} \tag{25}$$

In equation (25) r_w and r_e are the values of the radius at the wall and edge of the boundary layer, respectively. At the edge of the boundary layer the terms, u_e, w_e and p_e, are connected by the Bernoulli equation

$$p_\infty/\rho + 0{\cdot}5U_\infty^2 = p_e/\rho + 0{\cdot}5u_e^2 + 0{\cdot}5w_e^2. \tag{26}$$

The Dorodnitsyn formulation follows similar steps to those outlined in Section 2.1. First the independent variables (x, r) are transformed to (ξ, η) by defining

$$\xi = x \quad \text{and} \quad \eta = Re^{1/2}u_e(r_w - r). \tag{27}$$

New dependent variables are formed by

$$u' = u/u_e, \quad v' = Re^{1/2}v/u_e, \quad w' = w/u_e \quad \text{and} \quad q = p_e - p.$$

With the aid of the weight function, $f_k(u')$, the following composite equations are created:

$$f_k(u') \times \text{equation (20)} + (\mathrm{d}f_k/\mathrm{d}u') \times \text{equation (21)} = 0, \tag{28}$$

and

$$f_k(u') \times (w' \times \text{equation (20)} + \text{equation (23)}) + w'(\mathrm{d}f_k/\mathrm{d}u') \times \text{equation (21)} = 0. \tag{29}$$

Equations (28) and (29) are integrated across the boundary layer and the variable of integration changed from η to u'. With the restriction that $f_k(1) = 0$, the result is (dropping the superscripts $'$)

$$\frac{\partial}{\partial\xi}\left\{\int_0^1 u f_k \Theta \,\mathrm{d}u\right\} - Re^{1/2}u_e F|f_k|_{u=0} = u_{e\xi}^* \int_0^1 \frac{\mathrm{d}f_k}{\mathrm{d}u}\Theta(1-u^2)\,\mathrm{d}u + \frac{1}{u_e^2}\int_0^1 \frac{\mathrm{d}f_k}{\mathrm{d}u} Q\Theta \,\mathrm{d}u$$
$$+ u_e \int_0^1 \frac{\mathrm{d}f_k}{\mathrm{d}u}\frac{\partial}{\partial u}\{(1 + v_x/v)\mathrm{T}\}\,\mathrm{d}u - \frac{1}{Re^{1/2}}\left[\int_0^1 \frac{\mathrm{d}f_k}{\mathrm{d}u}\frac{(1+v_x/v)}{r}\,\mathrm{d}u + \int_0^1 f_k\left(\frac{v}{r\mathrm{T}}\right)\mathrm{d}u\right], \tag{30}$$

and

$$\frac{\partial}{\partial\xi}\left\{\int_0^1 uw f_k \Theta \,\mathrm{d}u\right\} = u_{e\xi}^* \int_0^1 w\frac{\mathrm{d}f_k}{\mathrm{d}u}\Theta(1-u^2)\,\mathrm{d}u + \frac{1}{u_e^2}\int_0^1 w\frac{\mathrm{d}f_k}{\mathrm{d}u} Q\Theta \,\mathrm{d}u$$
$$+ u_e\left\{\int_0^1 w\frac{\mathrm{d}f_k}{\mathrm{d}u}\frac{\partial}{\partial u}\left\{(1+v_x/v)\mathrm{T}\right\}\mathrm{d}u - u_{e\xi}^*\int_0^1 uw f_k\Theta\mathrm{d}u + u_e\int_0^1 f_k\frac{\partial}{\partial u}\left\{\frac{\partial w}{\partial u}(1+v_\phi/v)\mathrm{T}\right\}\mathrm{d}u\right.$$
$$\left. - \frac{1}{Re^{1/2}}\left[\int_0^1 w\frac{\mathrm{d}f_k}{\mathrm{d}u}\frac{(1+v_x/v)}{r}\,\mathrm{d}u + \int_0^1 f_k\frac{\partial w}{\partial u}\frac{(1+v_\phi/v)}{r}\,\mathrm{d}u + 2\int_0^1 f_k\left(\frac{vw}{r\mathrm{T}}\right)\mathrm{d}u\right], \tag{31}$$

where

$$u_{e\xi}^* \equiv \{\mathrm{d}u_e/\mathrm{d}\xi\}/u_e + w_e\{\mathrm{d}w_e/\mathrm{d}\xi\}/u_e^2, \tag{32a}$$

and

$$Q = \partial q/\partial\xi + [(r_w - r)u_{e\xi}^* + \mathrm{d}r_w/\mathrm{d}x][u_e^2w^2/r - w_e^2/r_e]. \tag{32b}$$

There is a clear structural similarity between equation (30) and equation (11). In equations (30) and (31) T, Θ, v, w and q are dependent variables and x and u are independent variables. As before

$$\mathrm{T} = 1/\Theta = \partial u/\partial\eta.$$

The pressure variation across the boundary layer is given by equation (22) manipulated into the form

$$\int_0^1 \frac{\mathrm{d}f_k}{\mathrm{d}u} q\,\mathrm{d}u + |f_k q|_{u=0} = -\frac{u_e}{Re^{1/2}}\int_0^1 f_k\Theta\left\{\frac{w^2}{r} - \frac{w_e^2/u_e^2}{r_e}\right\}\mathrm{d}u, \tag{33}$$

and v is obtained by integrating equation (20) across the boundary layer. The algebraic form chosen for the eddy viscosities, v_x and v_ϕ, is given in Section 3.3.

Equations (30) and (31) are the Dorodnitsyn equations for swirling internal boundary layer flow. Once approximate solutions have been introduced for T and Θ etc. and $f_k(u)$, chosen, the result is a system of ordinary differential equations in ξ.

3.2. *Dorodnitsyn finite element formulation*

The formulation is a straightforward extension of that described in Section 2.2. Approximate solutions for Θ and $(1+v_x/v)\mathrm{T}$ are given by equations (12) and (13) and $f_k(u)$ is given by equation (14). In addition the group formulation[20] is used to represent the various groups, e.g. $(1+v_x/v)/r$, that appear in equations (30) and (31). Substitution of the various approximate solutions and the weight function into equations (30), (31) and (33) gives the following ordinary differential equations:

$$\sum_j \mathrm{CC}_{kj}\mathrm{d}\theta_j/\mathrm{d}\xi = Re^{1/2}u_e F\delta_{1k} + u^*_{e\xi}\sum_j \mathrm{EF}_{kj}\theta_j + \frac{1}{u_e^2}\sum_j \mathrm{GG}_{kj}Q_j\theta_j$$
$$+ u_e\sum_j \mathrm{AA}_{kj}\{(1+v_x/v)\tau\}_j - \left[\sum_j \mathrm{EF}_{kj}\left\{\frac{v\theta}{r}\right\}_j + \sum_j \mathrm{GG}_{kj}\left\{\frac{1+v_x/v)}{r}\right\}_j\right]Re^{1/2}, \tag{34}$$

$$\sum_j \mathrm{CC}_{kj}\mathrm{d}(w\theta)_j/\mathrm{d}\xi = u^*_{e\xi}\sum_j(\mathrm{EF}_{kj}-\mathrm{CC}_{kj})(w\theta)_j + \frac{1}{u_e^2}\sum_j \mathrm{GG}_{kj}(wQ\theta)_j$$
$$+ u_e\sum_j \mathrm{GG}_{kj}\left[w\frac{\partial}{\partial u}\{(1+v_x/v)\tau\}\right]_j + u_e\sum_j \mathrm{FF}_{kj}\left\{\frac{\partial w}{\partial u}(1+v_\phi/v)\tau\right\}_j \tag{35}$$
$$-\left[\sum_j \mathrm{GG}_{kj}\{(1+v_x/v)w/r\}_j + \sum_j \mathrm{BB}_{kj}\left\{\frac{\partial w}{\partial u}\frac{(1+v_\phi/v)}{r}\right\}_j + 2\sum_j \mathrm{EE}_{kj}\{vw\theta/r\}_j\right]Re^{1/2},$$

and

$$\sum_j \mathrm{GG}_{kj}q_j + \delta_{1k}q_1 = -\frac{u_e}{Re^{1/2}}\sum_j \mathrm{EE}_{kj}\theta_j\left\{\frac{w^2}{r} - \frac{(w_e/u_e)^2}{r_e}\right\}. \tag{36}$$

Some of the coefficients given in equations (34)–(36) are evaluated by equation (16). The rest are evaluated from

$$\mathrm{GG}_{kj} = \int_0^1\left\{(1-u)\frac{\partial N_k}{\partial u} - N_k\right\}N_j\,\mathrm{d}u, \quad \mathrm{FF}_{kj} = \int_0^1 N_k(1-u)\left\{(1-u)\frac{\partial N_j}{\partial u} - N_j\right\}\mathrm{d}u,$$
$$\mathrm{BB}_{kj} = \int_0^1\left\{\frac{\partial N_k}{\partial u} - \frac{N_k}{1-u}\right\}N_j\,\mathrm{d}u \quad \text{and} \quad \mathrm{EE}_{kj} = \int_0^1 N_kN_j\,\mathrm{d}u. \tag{37}$$

Marching algorithms are constructed from equations (34) and (35) by introducing the approximation given by equation (17). After linearization of RHS^{n+1} about the downstream location, ξ_n, the final system of equations (equivalent to equation (18)) can be written

$$\sum_j\{\alpha\mathrm{CC}_{kj} - \beta\Delta\xi\,\partial\mathrm{RHS}_{34}/\partial\theta\}\Delta\theta_j^{n+1} = \Delta\xi\,\mathrm{RHS}_{34}^{n,\beta} - (1-\alpha)\sum_j \mathrm{CC}_{kj}\Delta\theta_j^n, \tag{38}$$

and

$$\sum_j\{\alpha\mathrm{CC}_{kj} - \beta\Delta\xi\,\partial\mathrm{RHS}_{35}/\partial(w\theta)\}\Delta(w\theta)_j^{n+1} = \Delta\xi\,\mathrm{RHS}_{35}^{n,\beta} - (1-\alpha)\sum_j \mathrm{CC}_{kj}\Delta(w\theta)_j^n. \tag{39}$$

As with equation (18), equations (38) and (39) are each tridiagonal or pentadiagonal systems that

can be solved efficiently using a generalized Thomas algorithm[4] to march from downstream location, ξ_n, to ξ_{n+1}. Since w does not appear in equation (38), it is convenient, at each step, to solve sequentially equation (38) for θ_j, equation (39) for w_j, equation (36) for q_j and to integrate equation (20) across the boundary layer to give v. For the solutions given in Section 4 the values $\alpha = 1{\cdot}5$, $\beta = 1{\cdot}0$ have been used in equations (38) and (39), which produces a stable second-order marching scheme. As the solution develops in the ξ direction the downstream step size, $\Delta\xi$, is adjusted using the same mechanism as described by Fletcher and Fleet.[10]

3.3. *Turbulence model*

As is clear from equations (21) and (23) eddy viscosities are introduced to represent the axial and circumferential Reynolds shear stresses. Here the two-layer representation for the eddy viscosity given by Cebeci and Smith[1] is extended to include the effect of swirl.

In the outer region a Clauser-type formulation is used:

$$(\nu_x/\nu)_0 = (\nu_\phi/\nu)_0 = 0{\cdot}0168 u_e R_e \delta_q^*/L, \tag{40}$$

where δ_q^* is the displacement area based on the total velocity. That is

$$\delta_q^* = \int_{r_e}^{r_w} r(1 - q_t/q_{te})\,\mathrm{d}r, \tag{41}$$

and

$$q_t^2 = u^2 + w^2, \quad q_{te}^2 = u_e^2 + w_e^2.$$

In the inner region the assumption of a balance between the production of turbulent energy and dissipation leads to the following expression for the axial eddy viscosity:

$$\nu_x = \frac{r}{r_w} l_x^2 [(\partial u/\partial r)^2 + (1/\sigma)(r\partial(w/r)/\partial r)^2]^{1/2}, \tag{42}$$

where $\sigma = \nu_x/\nu_\phi$ and the mixing length, l_x, is given by

$$l_x = \kappa r_w \ln(r_w/r)[1 - \exp\{-r_w \ln(r_w/r)\tau_{xw}^{1/2}/\rho^{1/2}A\}]. \tag{43}$$

Equation (43) contains the thick axisymmetric boundary layer correction due to Cebeci.[21] In equation (42) τ_{xw} is the wall value of the axial shear stress, the Von Karman constant $\kappa = 0{\cdot}41$ and A contains a pressure gradient correction,

$$A = \frac{26\nu}{\{1 - 21[u_e^2 u_{e\xi}^* \nu/(\tau_{xw}/\rho)^{3/2}]\}}. \tag{44}$$

Based on the numerical experimentation with two-dimensional turbulent wall-injection flows,[13] the parameter A contains no wall-injection correction.

In a manner similar to Koosinlin and Lockwood[22] it is postulated that, in the inner region

$$\nu_\phi = \frac{r}{r_w} l_\phi^2 [(\partial u/\partial r)^2 + (1/\sigma)(r\partial(w/r)/\partial r)^2]^{1/2}, \tag{45}$$

and

$$l_\phi = \kappa r_w \ln(r_w/r)[1 - \exp\{-r_w \ln(r_w/r)\tau_{\phi w}^{1/2}/\rho^{1/2}A\}], \tag{46}$$

where $\tau_{\phi w}$ is the wall value of the circumferential shear stress.

It may be noted that the above turbulence model degenerates to a conventional two-layer model when swirl is not present. The above model permits anisotropy in the eddy viscosities to appear

through the directional wall shear stresses used in the van Driest damping factor. This effectively limits the anisotropy to the viscous sublayer.

4. RESULTS AND DISCUSSION

The Dorodnitsyn finite element formulation (DOROD-FEM) described in Section 3 has been applied to swirling boundary layer flow in circular duct entries and in a 10 degree included-angle conical diffuser. For both cases blowing and suction in the normal direction at the wall have also been considered. All the results presented in this section have been obtained with ten linear elements (i.e. 11 grid points) spanning the boundary layer.

4.1. Duct entry flow

Experimental results due to Barbin and Jones[23] and Yeh[24] are available for the geometry shown in Figure 2. The data obtained by Barbin and Jones did not include the effects of swirl and have been used here to check the present method for non-swirling axisymmetric flow. As is clear from the velocity profiles shown in Figure 3 DOROD-FEM produces solutions in good agreement with the experimental results. The Reynolds number for these results is $Re = 0{\cdot}399 \times 10^6$. The co-ordinate x in Figure 3 and all subsequent Figures is equivalent to ξ in Section 3. The co-ordinate y in Figure 3 is measured from the wall in the radial direction.

The experimental data of Yeh[24] were obtained in an annulus rather than a duct. However the boundary layer development on the inner surface of the outer annulus wall is the same as for a duct. Yeh considered both swirling and non-swirling entry flow but only presented velocity measurements at two downstream stations corresponding to $x/L = 1{\cdot}50$ and $2{\cdot}50$ in Figure 2. The Reynolds number, based on L and u_e at $x/L = 1{\cdot}50$, is $Re = 0{\cdot}994 \times 10^6$. A comparison of the axial circumferential velocity distributions at $x/L = 2{\cdot}50$ is shown in Figure 4. Good agreement between the computational (DOROD-FEM) and experimental (YEH) results is indicated.

For both the Barbin and Jones case and the Yeh case the axial pressure gradient is slightly negative, i.e. slightly favourable. The variation of the axial skin friction coefficient corresponding to Yeh's experiments is shown in Figure 5. It can be seen that the inclusion of swirl (at $x/L = 1{\cdot}5$, $w_e/u_e = 0{\cdot}4$) does not significantly alter the skin friction. However the introduction of blowing at the wall ($F \equiv v_w/u_e$) causes a marked reduction in the skin friction coefficient. The rapid adjustment in the skin friction between $x/L = 1{\cdot}50$ and $1{\cdot}60$ is due to the use of the experimental (non-blowing) velocity profiles to start the computation at $x/L = 1{\cdot}50$. Consequently the skin friction variation shown in Figure 5 indicates the response of the boundary layer to the sudden initiation of blowing at $x/L = 1{\cdot}50$. The blowing rate is constant at $F = 0{\cdot}002$ for $1{\cdot}50 \leqslant x/L \leqslant 2{\cdot}50$.

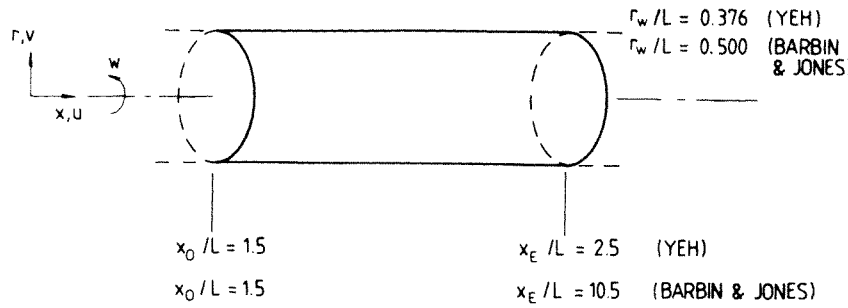

Figure 2. Duct entry boundary layer flow

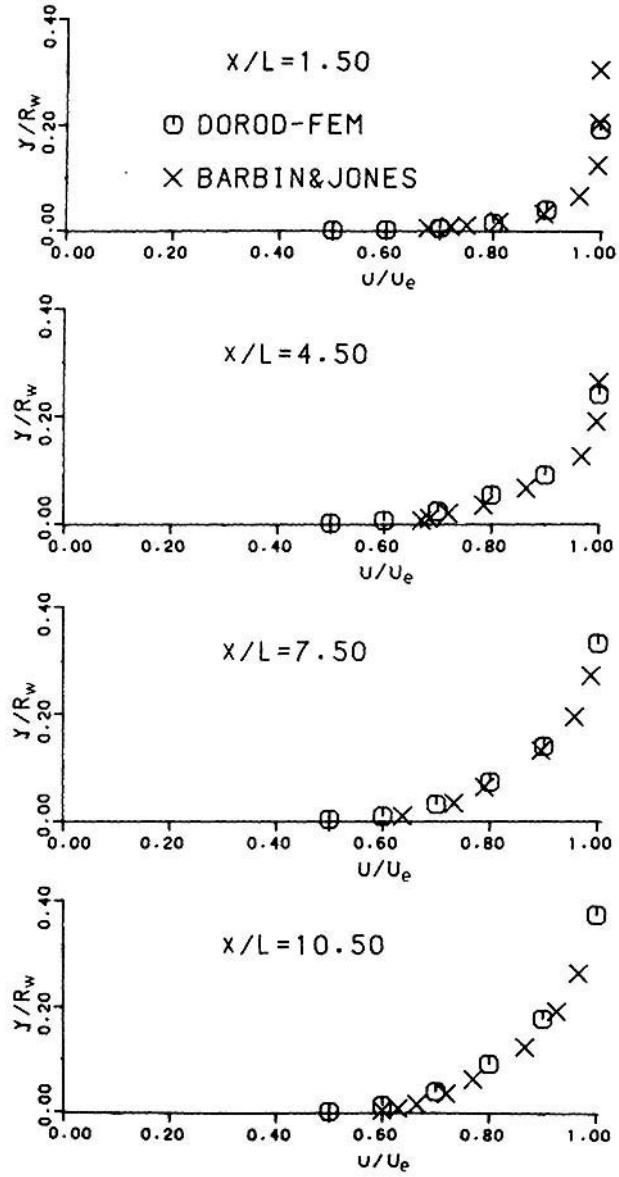

Figure 3. Velocity profiles for duct entry flow

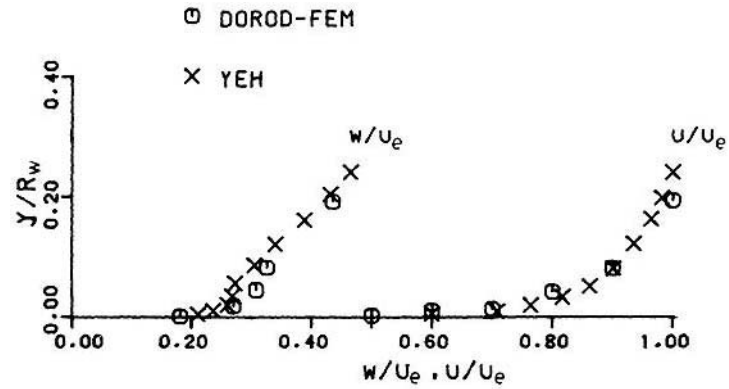

Figure 4. Velocity distributions at $x/L = 2{\cdot}50$

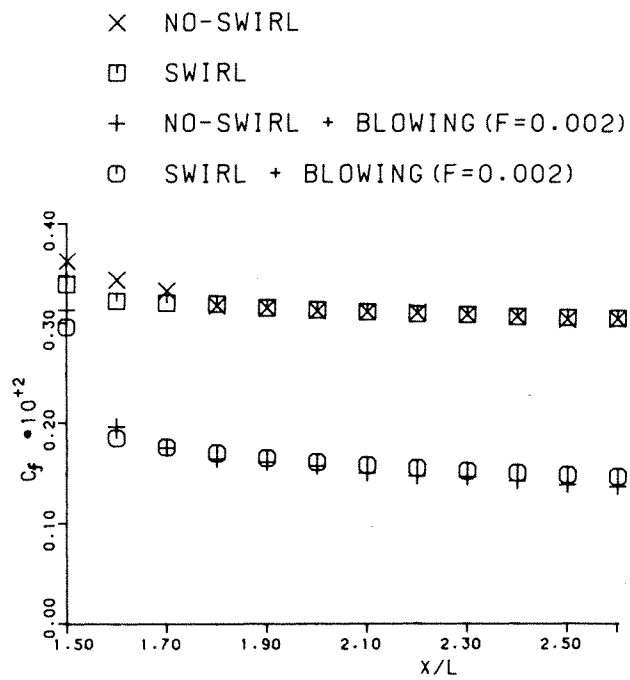

Figure 5. Skin friction variation for duct entry flow

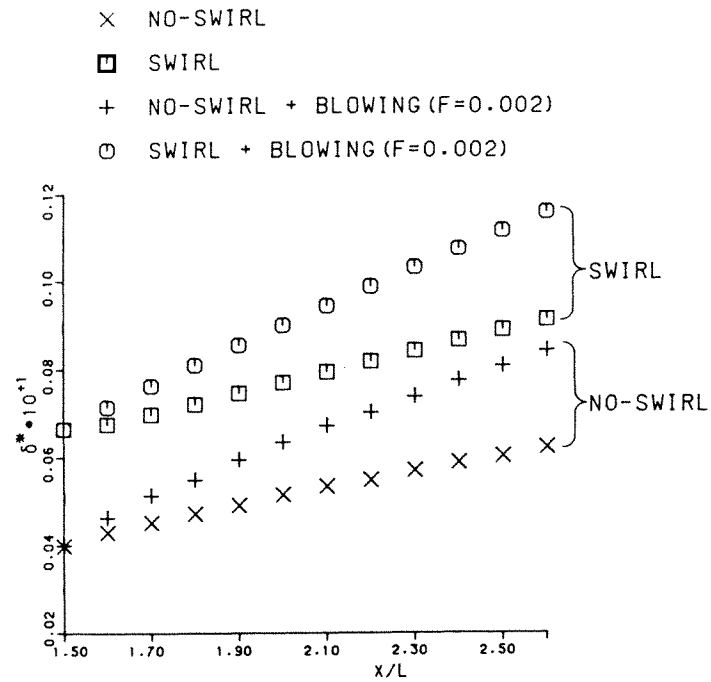

Figure 6. Displacement area variation for duct entry flow

The corresponding variation in axial displacement area is shown in Figure 6. The axial displacement area is defined by

$$\delta^* = \int_{r_e}^{r_w} r(1-u)\,dr. \tag{47}$$

It is expected that the response of the boundary layer thickness to swirl and wall injection will be qualitatively similar to that of the axial displacement area.

It may be noted that the swirl and non-swirl cases have started from the corresponding experimental velocity distributions, and consequently have different displacement areas at $x/L = 1{\cdot}50$. As with the axial skin friction behaviour, swirl has relatively little influence on the growth in displacement area. However the inclusion of blowing causes a rapid growth in displacement area in the downstream direction and, by implication, in the boundary layer thickness.

Although not shown in Figures 5 and 6 the introduction of suction ($F = -0{\cdot}002$) causes an increase in skin friction and a decrease in the rate of growth of the displacement area.

4.2. *Conical diffuser flow*

Fraser[25] has made measurements of the velocity distribution and deduced skin friction and displacement area behaviour for the flow in a 10 degree included-angle conical diffuser (Figure 7). Fraser's experiments included neither swirl nor wall injection. To investigate the influence of swirl it has been necessary to make assumptions about the upstream profile, $w_i(r)$, and the boundary layer edge variation, $w_e(x)$, of the circumferential velocity component. The downstream solution for the duct entry case has provided the upstream profile, $w_i(r)$. The boundary layer edge velocity, has been obtained by assuming that angular momentum is conserved and that the inviscid circumferential velocity is vortex-like, i.e.

$$w_e r_e = (w_e r_e)_{x_0} \quad \text{and} \quad w_e = k/r_e. \tag{48}$$

A consideration of the inviscid circumferential momentum equation (left-hand side of equation (23) set equal to zero), indicates that $\partial w_e/\partial x = 0$, so that $u^*_{e\xi} = \{du_e/d\xi\}/u_e$ (see equation (31a)).

The diffuser section starts at $x/L = 1{\cdot}50$ so that up to this point the axial pressure gradient is slightly negative. Downstream of $x/L = 1{\cdot}50$ the axial pressure gradient is positive (see Figure 8). The Reynolds number of Fraser's experiment and the present computation is $Re = 0{\cdot}386 \times 10^6$ based on L and u_e at $x/L = 1{\cdot}0$.

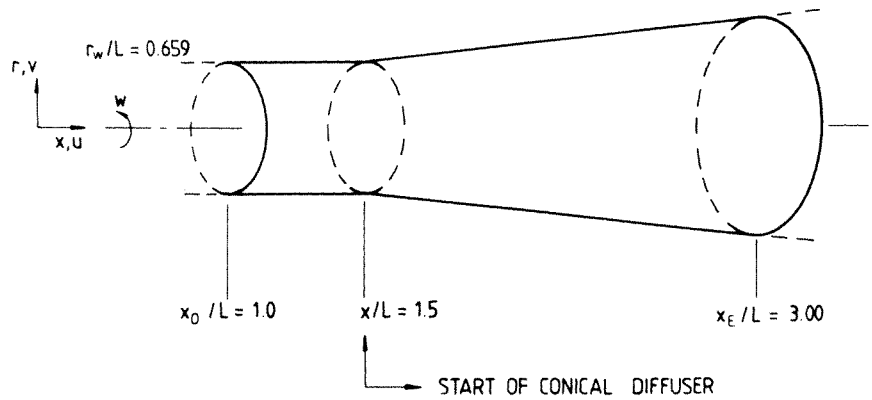

Figure 7. Conical diffuser geometry

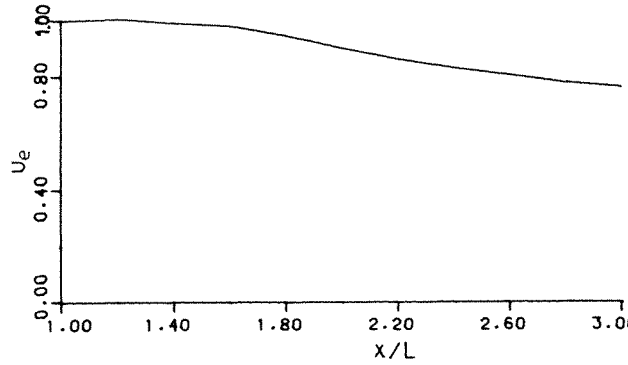

Figure 8. Axial velocity distribution at boundary layer edge

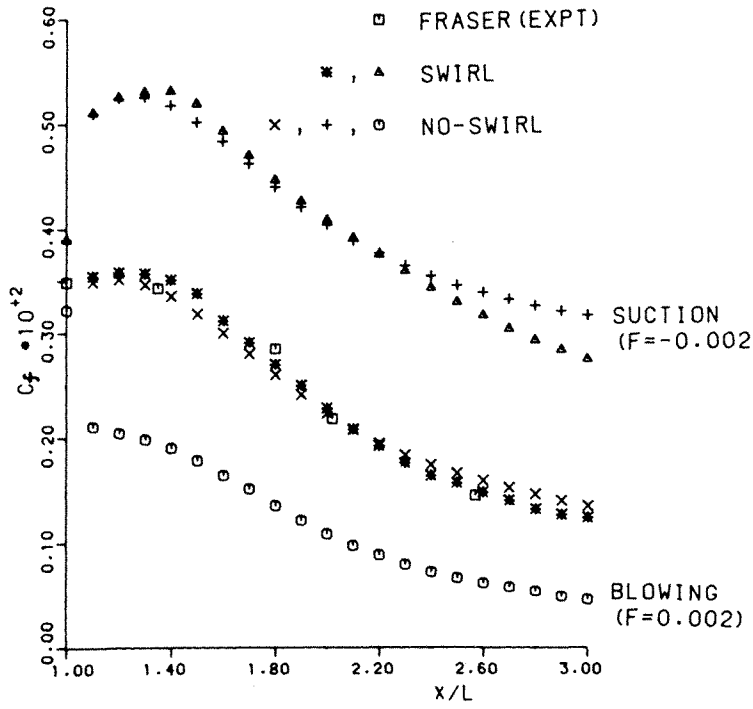

Figure 9. Axial skin friction variation for conical diffuser

The axial skin friction variation with axial position is shown in Figure 9. Included in Figure 9 are the values of skin friction coefficient deduced by Fraser from the experimental velocity distributions. It is apparent that good agreement is obtained between the experimental and computed results.

It is of interest that the inclusion of swirl (at $x/L = 1{\cdot}0$, $w_e/u_e = 0{\cdot}4$) causes relatively little change in the skin friction. For small values of x/L the introduction of swirl causes a slight increase in axial skin friction. However, in the adverse pressure gradient regime ($x/L \geqslant 1{\cdot}50$) the effect of swirl is to eventually cause a reduction in axial skin friction compared with the no-swirl case. This is more pronounced when suction is also applied. The data shown in Figure 9 indicate that blowing and

suction are both more effective in altering the skin friction behaviour than is the introduction of swirl.

The variation of displacement area with axial position is shown in Figure 10. Good agreement with the experimental data of Fraser (nonswirling flow with no blowing or suction) is indicated for small values of x/L. For large values of x/L the computational results slightly underpredict the experimental data.

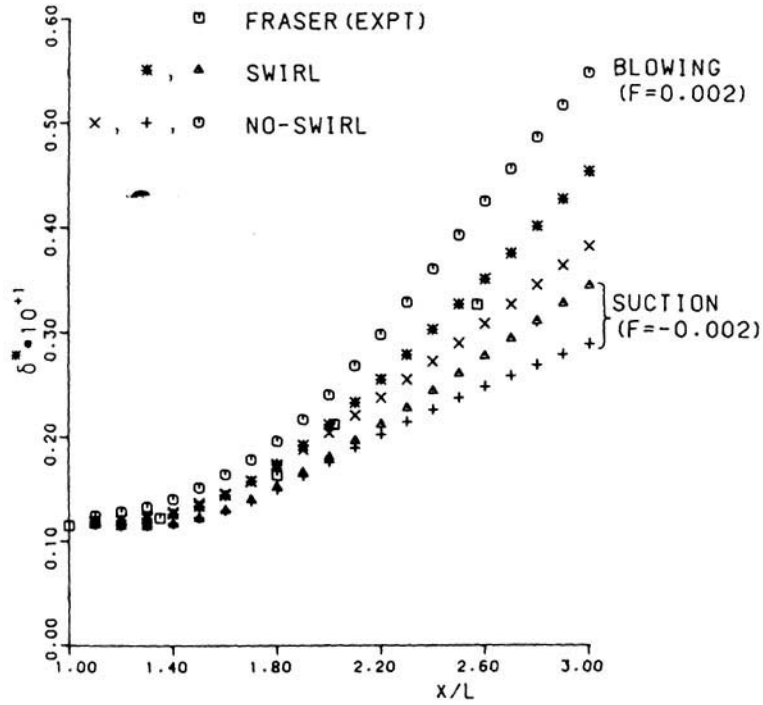

Figure 10. Displacement area variation for conical diffuser

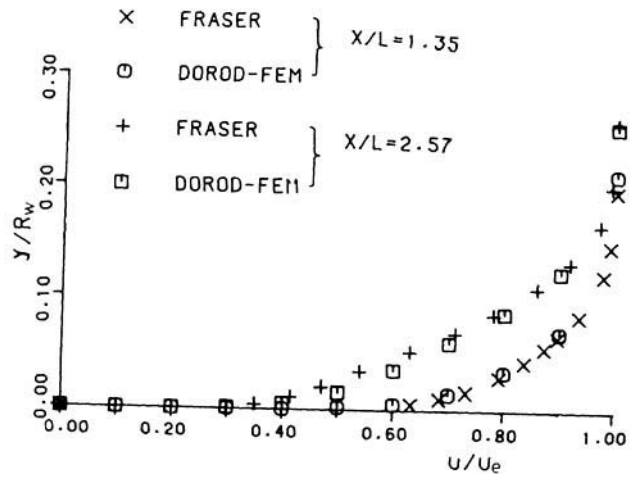

Figure 11. Velocity distribution comparison for non-swirling flow

In contrast to the behaviour in a slightly negative pressure gradient (Figure 6) the present results (Figure 10) indicate that the inclusion of swirl causes a noticeable increase in displacement area growth. It is surmised that the increased turbulent mixing associated with swirl is not as effectively suppressed by the adverse pressure gradient. The introduction of blowing or suction is seen to have a marked effect on displacement area growth.

For the non-swirl case, with no suction or blowing, typical axial velocity distributions are compared with the corresponding experimental results of Fraser in Figure 11. Good agreement is indicated. The adverse pressure gradient has reduced the axial velocity, particularly close to the wall, and has clearly caused a thickening of the boundary layer in the downstream direction.

The velocity distribution at $x/L = 1{\cdot}35$ is plotted on a semilog scale in Figure 12(a) to examine the behaviour near to the wall more closely. The co-ordinates u^+ and y^+ are defined by

$$u^+ = u(\tau_{xw}/\rho)^{1/2} \quad \text{and} \quad y^+ = (\tau_{xw}/\rho)^{1/2}(r_w - r)/\nu. \tag{49}$$

It is clear that the addition of swirl to the flow does not significantly alter the axial velocity profile, whereas the introduction of suction causes a substantial change in the velocity profile while still retaining an essentially semi-logarithmic behaviour. A similar pattern is apparent for the velocity distribution at $x/L = 2{\cdot}57$ (Figure 12(b)), however now the introduction of swirl is indicating a greater change than for $x/L = 1{\cdot}35$ but still as part of a unique relationship between u^+ and $\ln y^+$. As at $x/L = 1{\cdot}35$ the introduction of suction causes a different relationship to be produced, while still retaining the semi-logarithmic character.

The behaviour of the circumferential velocity distribution at the two downstream locations is shown in Figure 13. There is relatively little difference in the form of the velocity distributions indicating that the adverse axial pressure gradient has relatively little influence on the circumferential velocity behaviour. It is also clear that introducing suction has a very small effect. Compared with the axial velocity distribution shown in Figure 11, the circumferential velocity retains the 'inviscid' character until much closer to the wall.

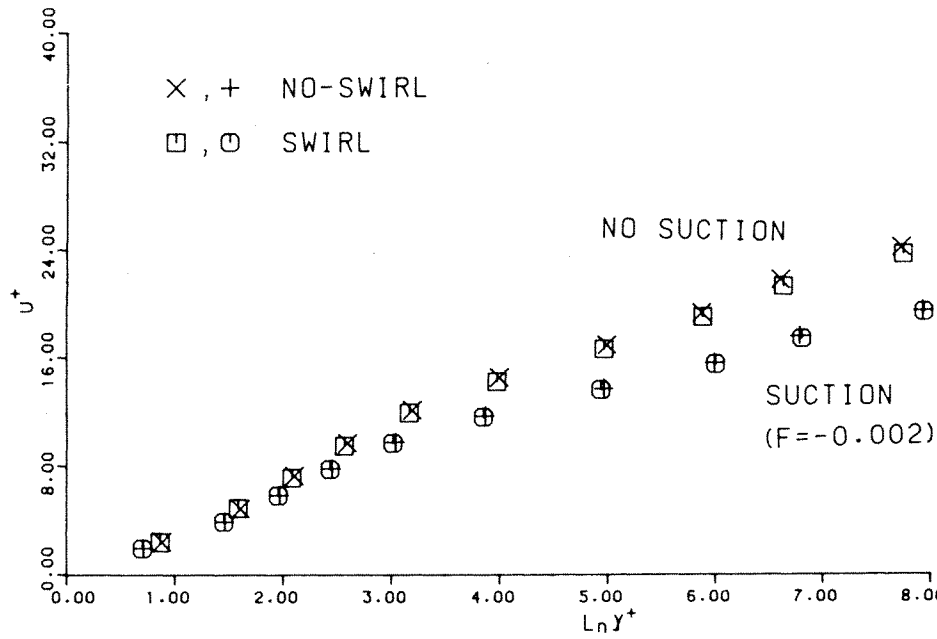

Figure 12(a). Axial velocity distribution at $x/L = 1{\cdot}35$

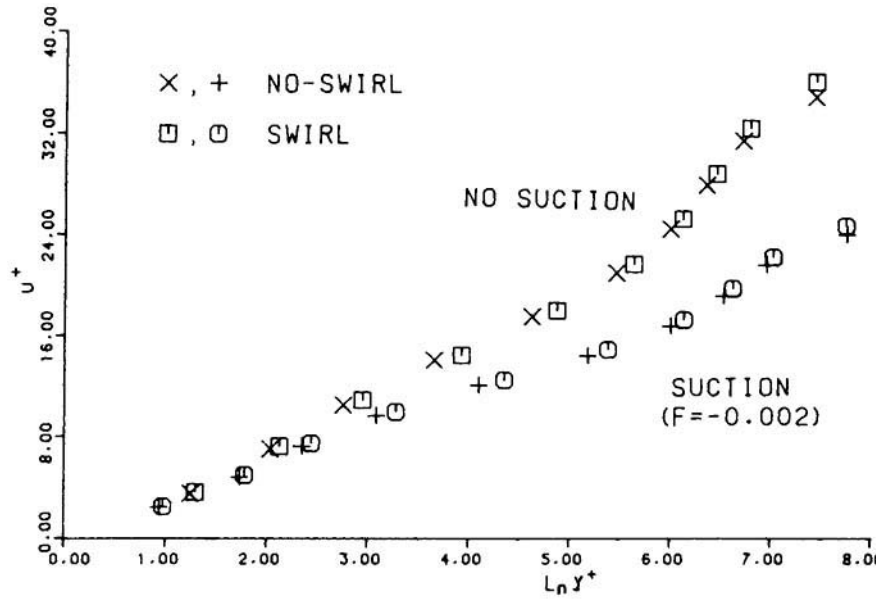

Figure 12(b). Axial velocity distribution at $x/L = 2{\cdot}57$

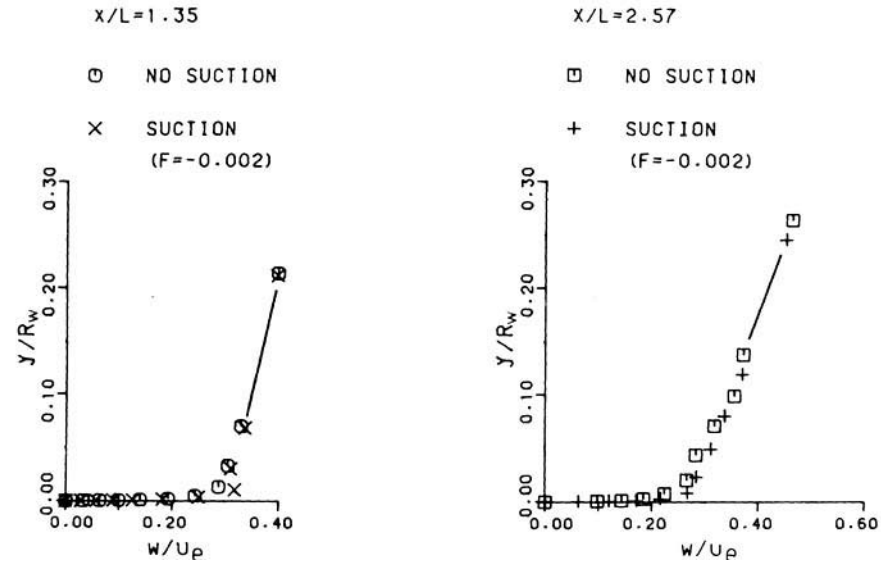

Figure 13. Circumferential velocity distribution for conical diffuser

The behaviour of the axial shear stress at the two downstream locations is shown in Figures 14(a) and 14(b).

At $x/L = 1{\cdot}35$ the axial shear stress demonstrates a monotonic behaviour, rising from zero at the edge of the boundary layer to a maximum at the wall. The introduction of swirl causes a slight increase in the axial shear stress at all locations in the radial direction. The introduction of suction increases the magnitude of the axial shear stress close to the wall without significantly altering the distribution of axial shear stress further from the wall.

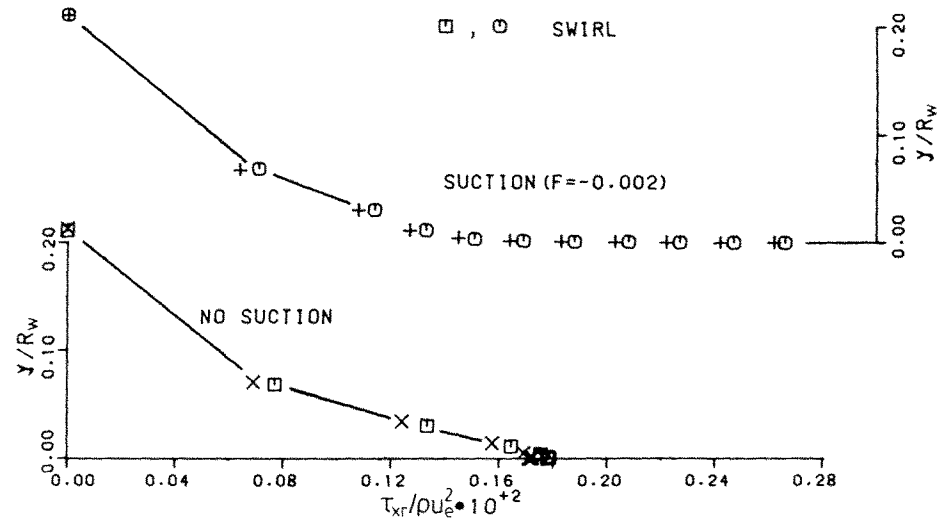

Figure 14(a). Axial shear stress distribution, $x/L = 1{\cdot}35$

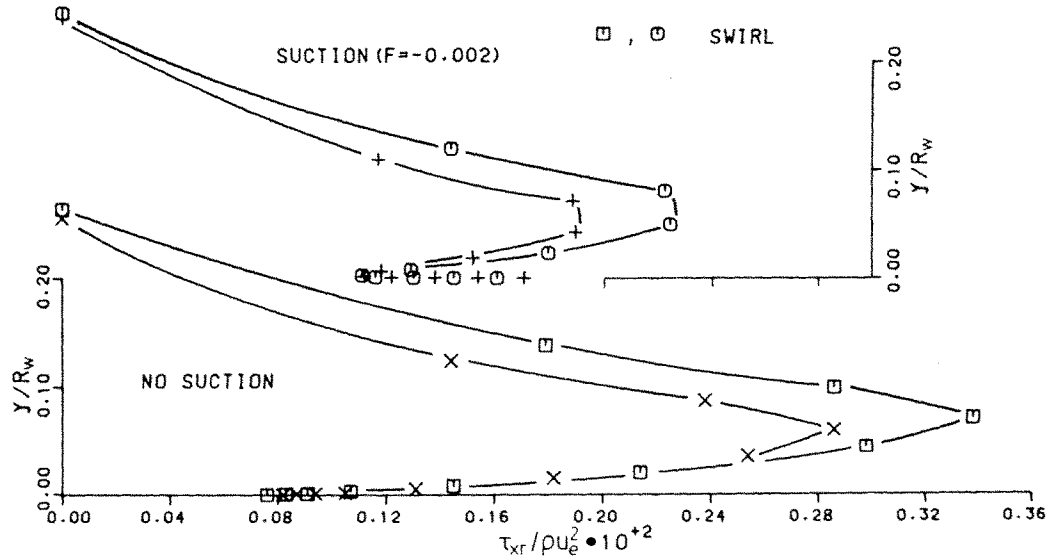

Figure 14(b). Axial shear stress distribution, $x/L = 2{\cdot}57$

The radial distribution of the axial shear stress at $x/L = 2{\cdot}57$ is substantially different, primarily due to the influence of the adverse pressure gradient. For the case of no swirl and no suction the axial shear stress increases to a maximum close to the wall and then falls sharply as the wall is approached. The addition to swirl increases the axial shear stress by a small amount everywhere except immediately adjacent to the wall. The addition of suction reduces the peak axial shear stress and also causes a local increase in the shear stress adjacent to the wall. There appears to be relatively little interaction between suction and swirl.

The circumferential shear stress distribution is shown in Figure 15. In contrast to the situation for the axial shear stress, the distribution of the circumferential shear stress at the two downstream

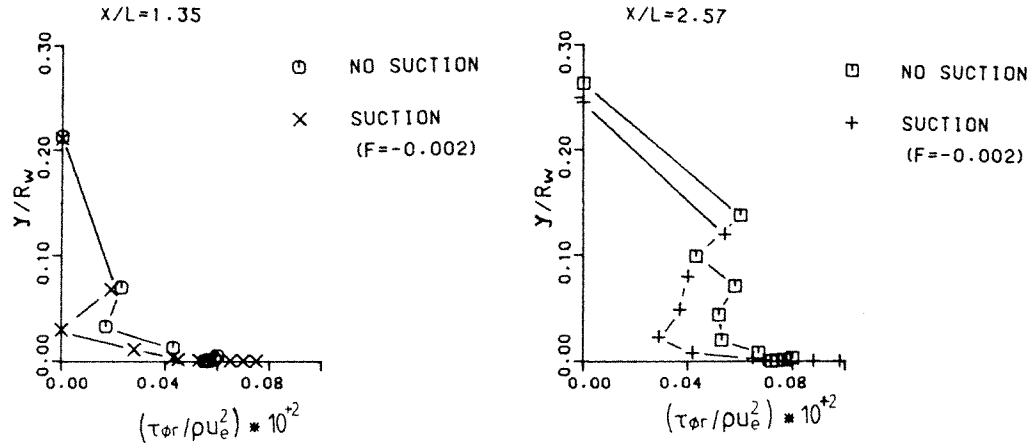

Figure 15. Circumferential shear stress distribution

locations is very similar. The implied lack of dependence on the axial pressure gradient was also apparent in the circumferential velocity distributions (Figure 13). The circumferential shear stress increases rapidly as the wall is approached. The additional influence of suction is to reduce the circumferential shear stress close to the wall with a corresponding increase at the wall.

The relative independence of the circumferential flow behaviour in relation to the axial flow behaviour has also been observed for swirling flow through annular conical diffusers.[26]

Since the wall values of the axial and circumferential shear stresses are proportional to the normal gradients of the corresponding velocity components, it follows that the direction of the resultant shear stress at the wall is the same as the direction of the limiting streamline at the wall.

Comparing Figures 14(a), 14(b) and 15 indicates that the adverse pressure gradient acts to significantly reduce the axial shear stress at the wall while leaving the circumferential shear stress at the wall relatively unaffected, in the absence of suction. This implies that the resultant shear stress, and hence the total velocity close to the wall, swings towards the circumferential direction in moving downstream. Eventually the axial shear stress will become negative and the resultant shear stress will be directed upstream. However this implies that the axial velocity component will be negative adjacent to the wall.

The current form of the Dorodnitsyn formulation, equations (30) and (31), requires that axial velocity component, u, is monotonic with η. To extend the present formulation beyond the point where u becomes negative would require splitting the boundary layer into an inner layer and an outer layer, in each of which u is monotonic with η. This procedure has been used with the traditional Dorodnitsyn method[5] but is not attempted here.

5. CONCLUSION

The Dorodnitsyn finite element formulation has been extended to swirling internal turbulent boundary layer flow with blowing or suction in the radial direction at the wall. Computed solutions agree well with the experimental measurements of duct entry flows by Barbin and Jones[23] and Yeh[24] and with the conical diffuser flow of Fraser.[25] The inclusion of swirl, $(w_e/u_e)_i = 0{\cdot}4$, has relatively little influence on such boundary layer parameters as axial skin friction and displacement area when there is a slight negative pressure gradient. By contrast blowing, with $v_w/u_e = 0{\cdot}002$, causes a significant reduction in the axial skin friction and a rapid growth in the displacement area. For an adverse pressure gradient, as occurs in the diffuser, the addition of swirl has little influence

on the axial skin friction but does produce an increase in the rate of growth of displacement area. The circumferential velocity and shear stress components are relatively unaffected by the adverse pressure gradient; consequently the limiting streamline at the surface becomes parallel to the circumferential direction at some downstream location. For an adverse pressure gradient the influence of the suction is limited to the region adjacent to the wall.

ACKNOWLEDGEMENTS

The author is grateful to Dr. K. Srinivas for his assistance in preparing the figures.

This research is part of an investigation of internal swirling flows supported by the Australian Research Grants Scheme.

REFERENCES

1. T. Cebeci and A. M. O. Smith, *Analysis of Turbulent Boundary Layers*, Academic Press, New York, 1974.
2. P. Coles and E. Hirst (eds), *Computation of Turbulent Boundary Layer—1968, AFORSR-ISP Stanford Conference*, 1968.
3. A. A. Dorodnitsyn, 'General method of integral relations and its application to boundary layer theory', *Adv. Aero. Sci.*, **3**, 207–219 (1962).
4. C. A. J. Fletcher, *Computational Galerkin Methods*, Springer-Verlag, New York, 1984, p. 175.
5. M. Holt, *Numerical Methods in Fluid Dynamics*, Springer-Verlag, Heidelberg, 1977.
6. C. A. J. Fletcher, 'Application of an improved method of internal relations to the supersonic boundary layer flow about cones at large angles of attack', in J. Noye (ed.), *Numerical Simulation of Fluid Motion*, North-Holland, 1978, pp. 537–550.
7. C. A. J. Fletcher and M. Holt, 'An improvement to the method of integral relations, *J. Comp. Phys.*, **18**, 154–164 (1975).
8. C. A. J. Fletcher and M. Holt, 'Supersonic flow about inclined cones', *J. Fluid Mech.*, **74**, 561–591 (1976).
9. W. -S. Yeung and R. -J. Yang, 'Application of the method of integral relations to the calculation of two-dimensional incompressible turbulent boundary layers', *J. Appl. Mech.*, **48**, 701–706 (1981).
10. C. A. J. Fletcher and R. W. Fleet, 'A Doronitsyn finite element formulation for turbulent boundary layers', *Comp. and Fluids*, **12**, 31–45 (1984).
11. R. W. Fleet and C. A. J. Fletcher, 'Application of the Dorodnitsyn boundary layer formulation to turbulent compressible flow', *Eighth Australian Fluid Mechanics Conference*, Newcastle, Australia, November 1983, pp. 1C1–1C4.
12. C. A. J. Fletcher and R. W. Fleet, 'A Dorodnitsyn finite element formulation for laminar boundary layer flow', *Int. J. Num. Meth. Fluids*, **4**, 399–419 (1984).
13. C. A. J. Fletcher and R. W. Fleet, 'Turbulent boundary layers with mass transfer by the Dorodnitsyn finite element method, *J. Appl. Mech.* (to appear, 1985).
14. C. A. J. Fletcher, 'Computational analysis of diffuser-augmented wind turbines', *Energy Conv. and Magment.*, **21**, 175–184 (1981).
15. C. A. J. Fletcher and B. W. Roberts, 'Electricity generation from jet-stream winds', *J. Energy*, **3**, 241–249 (1979).
16. C. A. J. Fletcher, A. J. Honan and J. S. Sapuppo, 'Aerodynamic platform comparison for jet-stream electricity generation', *J. Energy*, **7**, 17–23 (1983).
17. Y. Senoo, N. Kawaguchi and T. Nagata, 'Swirl flow in conical diffusers', *Bull. JSME*, **21**, 112–119 (1978).
18. O. C. Zienkiewicz, *The Finite Element Method*, 3rd Edn., McGraw-Hill, London.
19. W. C. Reynolds, 'Computation of turbulent flows', *Ann. Rev. Fluid Mechanics*, **8**, 183–208 (1976).
20. C. A. J. Fletcher, 'The group finite element formulation', *Comp. Meth. Appl. Mech. Eng.*, **37**, 225–243 (1983).
21. T. Cebeci, 'Eddy-viscosity distribution in thick axisymmetric turbulent boundary layers', *J. Fluids Eng.*, **95**, 319–326 (1973).
22. M. L. Koosinlin and F. C. Lockwood, 'The prediction of axisymmetric turbulent swirling boundary layers', *AIAA J.*, **12**, 547–554 (1974).
23. A. R. Barbin and J. B. Jones, 'Turbulent flow in the inlet region of a smooth pipe', *J. Basic Eng.*, **85**, 29–34 (1963).
24. H. Yeh, 'Boundary layer along annular walls in a swirling flow', *Trans. ASME*, **80**, 767–776 (1958).
25. H. R. Fraser, *Proc. ASCE*, **84**, 1684/1–17 (1958), also see Reference 2.
26. R. P. Lohmann, S. J. Markowski and E. J. Brookman, 'Swirling flow through annular diffusers with conical walls', *J. Fluids Eng.*, **101**, 224–228 (1979).